Semnan University

Journal of Heat and Mass Transfer Research

Journal homepage: http://jhmtr.journals.semnan.ac.ir

The optimization of inlet and outlet port locations of a vented square cavity

Taher Armaghani[a],*, Farhad Talebi[b] , Amir Houshang Mahmoudi[b], Mahmoud Farzaneh Gord[c]

[a] *Islamic Azad University Mahdishahr Branch, Department of Engineering, Mahdishahr, Iran*
[b] *Department of Mechanical Engineering, Semnan University, Semnan, Iran*
[c] *Department of Mechanical Engineering, Shahrood University of Technology, Shahrood, Iran*

PAPER INFO

History:
Received 16 July 2013
Received in revised form
20 January 2014
Accepted 2 March 2014

Keywords:
Vented square cavity
Entropy Generation
Heat transfer
Irreversibility
Fluid friction
irreversibility

ABSTRACT

In this study, mixed convection heat transfer and local and global entropy generation in a ventilated square cavity have been investigated numerically. The natural convection effect is achieved by a constant heat flux imposed at the bottom wall and cooled by injecting a cold follow. In order to investigate the effect of port location, four different placement configurations of the inlet and outlet ports are studied. In each case, external flow enters into the cavity through an inlet port in the left side of the cavity and exits from the opposite side. The other boundaries are assumed adiabatic. The cavity is subjected to laminar flow of water. The investigation has been carried out for the Re=1000, and the Richardson number with the range of $0.0001<Ri<10$. The heat transfer and LEG (Local Entropy Generation) and GEG (Global Entropy Generation), Heat Transfer Irreversibility (HTI) and Fluid Friction Irreversibility (FFI) are calculated and compared. Then, the optimum inlet/outlet configuration has been selected based on the minimum GEG and the maximum heat transfer.

1. Introduction

Fluid flow and heat transfer in a ventilated cavity are presented in many transport processes in the nature and in the engineering devices. Indeed, the combination of forced and natural convections has been recommended for high heat dissipating electronic components, where natural convection is notable for providing effective cooling [1]. Significance of the mixed convection flow can be found in atmospheric flows, solar energy storage, heat exchangers, lubrication technology, drying technologies, and cooling the electronic devices. A brief review of literature [2-8] shows that, due to practical importance, the study of mixed convection heat transfer in the enclosures has attracted remarkable attention in the past few decades. Mahmoudi et al. [9] studied the effect of inlet and outlet ports' location in the mixed convection flow and heat transfer in a ventilated square cavity. For the cavity, it could be realized that many researches are focused on the enhanced heat transfer.

All the aforementioned studies are based on the first-law analyses. Recently, the second-law based investigations have been paid attention for studying thermal systems. Entropy generation has been used as a gauge to evaluate the performance of thermal system. The analysis of the exergy utilization and the entropy generation has become one of the primary objectives in designing a thermal system. Bejan [10-12] focused on the different reasons behind entropy generation in applied

Corresponding author: T. Armaghani, Ph.D., *Islamic azad university Mahdishahr branch, Department of engineering, Mahdishahr, Iran*
Email:*taherarmaghani@yahoo.com/ Fax: 02323623189*

thermal engineering. Generation of entropy destroys the current work of a system. Therefore, it makes a good engineering sense of focusing on irreversibility of heat transfer (HTI) and fluid flow (FFI) processes. Many investigators have studied entropy generation in natural, forced, and mixed convections [13-16]. Kasagi and Nishimura [13] studied the DNS of combined forced and natural convections on a vertical plane channel. Baytas [14] studied the natural convection heat transfer in porous media and investigated the entropy generation in the mentioned problem. Another investigation is the second-law analysis on fundamental convective heat transfer problem done by Mahmud and Fraser [15]. Omri and Nasrallah [17] considered mixed convection in an air-cooled cavity with differentially heated vertical isothermal sidewalls having inlet and exit ports by a control volume finite element method. They investigated two different placement configurations of the inlet and exit ports on the sidewalls. The best configuration was selected to analyze the cooling effectiveness of the cavity, which suggested that injecting air through the cold wall was more effective on removing heat and placing inlet near the bottom and exit near the top which produced effective cooling. Later, Singh and Sharif [18] extended their works by considering six placement configurations of the inlet and outlet of a differentially heated rectangular enclosure whereas the previous study was limited to only two different configurations of inlet and outlet ports. The problem of mixed convection heat transfer in a square cavity with a centered heat conducting horizontal square solid cylinder is analyzed by Rahman et al. [19]. Balaji et al. [20] investigated the entropy generation minimization in turbulent mixed convection flows. The importance of thermal boundary condition in heat transfer and entropy generation for natural convection inside a porous enclosure is investigated by Zahmatkesh [21]. Shahi et al. [22] reported entropy generation due to natural convection cooling of nanofluid. Recently Mahmoudi et al. [23] studied the MHD natural convection and entropy generation in a trapezoidal enclosure using nanofluid.

For the ventilated square cavity, one interesting question would be about the optimum location of the inlet and outlet ports in order to minimize entropy generation resulting in the best performance. Finding the optimal case and optimum design for engineering tools is very important.

The aim of this study is to investigate the effect of inlet and outlet locations on the mixed convection, local entropy generation, FFI (Fluid Friction Irreversibility), and HTI (Heat Transfer Irreversibility) in a ventilated square cavity based on a numerical analysis. Based on the second law analysis, the best configuration has been proposed in which entropy generation is minimized throughout the cavity. With regard to the mentioned aspects, numerical study is carried out over the wide range of Richardson number while the Reynolds number is kept constant at 1000. Figure 1 shows a schematic diagram of the cavity with various flow configurations of the current problem.

2. Problem definition and mathematical formulation

A two-dimensional square cavity considered for the this study is shown in fig. 1. In order to induce the buoyancy effect, the bottom horizontal wall has an embedded constant heat flux source, *q"*. Non-heated parts of the bottom wall and the remaining walls are insulated. The cavity is subjected to an external flow entering into the cavity located on the left vertical wall and leaving from the opposite vertical wall. The governing equations for the steady, two-dimensional laminar and incompressible mixed convection flow are expressed as following:

Continuity:

$$\frac{\partial u}{\partial x}+\frac{\partial v}{\partial y}=0 \tag{1}$$

Momentum:

$$u\frac{\partial u}{\partial x}+v\frac{\partial u}{\partial y}=-\frac{1}{\rho}\frac{\partial p}{\partial x}+\upsilon\left(\frac{\partial^2 u}{\partial x^2}+\frac{\partial^2 u}{\partial y^2}\right) \tag{2}$$

$$u\frac{\partial v}{\partial x}+v\frac{\partial v}{\partial y}=-\frac{1}{\rho}\frac{\partial p}{\partial y}+\upsilon\left(\frac{\partial^2 v}{\partial x^2}+\frac{\partial^2 v}{\partial y^2}\right)+g\beta\left(T-T_c\right) \tag{3}$$

Energy:

$$u\frac{\partial T}{\partial x}+v\frac{\partial T}{\partial y}=\alpha\left(\frac{\partial^2 T}{\partial x^2}+\frac{\partial^2 T}{\partial y^2}\right) \tag{4}$$

The local entropy generation (LEG) equation is given as [12]:

$$S_{gen}=\frac{k}{T^2}\left[\left(\frac{\partial T}{\partial x}\right)^2+\left(\frac{\partial T}{\partial y}\right)^2\right]+\frac{\mu}{T}\left[2\left\{\left(\frac{\partial u}{\partial x}\right)^2+\left(\frac{\partial v}{\partial y}\right)^2\right\}+\left(\frac{\partial u}{\partial y}+\frac{\partial v}{\partial x}\right)^2\right] \tag{5}$$

The comparison between efficient cooling in different configurations is done based on the average bulk fluid temperature in the cavity and the average Nusselt number at the heated surface. So, we calculate Nu_m (the average Nusselt number) at the heat source surface and the bulk average temperature as:

$$Nu_m=\frac{\int_0^w Nu(X)dX}{\int_0^w dX} \tag{6}$$

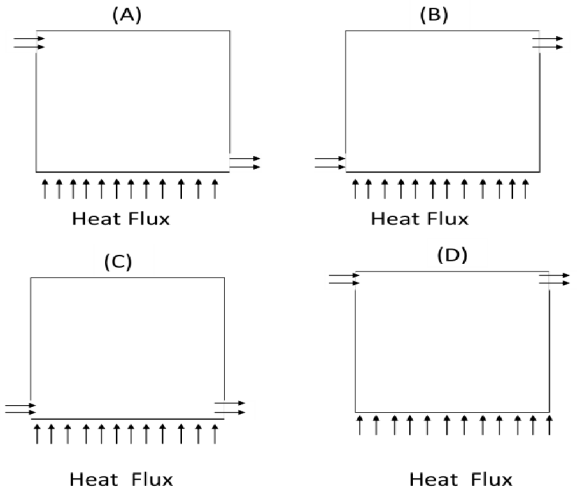

Figure 1) The vented square cavity under investigation A) TB configuration- B) BT configuration –C) BB configuration –D) TT configuration .

where $Nu(X)$ is defined as:

$$Nu(X)=\frac{1}{\theta(X)}$$
$$T_{av}=\frac{1}{V}\int TdV \tag{7}$$

where V is the cavity's volume.

Equations (1)-(4) can be converted to the dimensionless forms by definition of the following parameters:

$$X=\frac{x}{H},\ Y=\frac{y}{H},\ U=\frac{u}{U_0},\ V=\frac{v}{U_0},$$
$$\theta=\frac{T-T_c}{q''H/\ k_f},\ P=\frac{p}{\rho U^2{}_0} \tag{8}$$

Therefore, using the above parameters leads to dimensionless forms of the governing equations as below:

$$\frac{\partial U}{\partial X}+\frac{\partial V}{\partial Y}=0 \tag{9}$$

$$U\frac{\partial U}{\partial X}+V\frac{\partial U}{\partial Y}=-\frac{\partial P}{\partial X}+\frac{1}{\mathrm{Re}}\left(\frac{\partial^2 U}{\partial X^2}+\frac{\partial^2 U}{\partial Y^2}\right) \tag{10}$$

$$U\frac{\partial V}{\partial X}+V\frac{\partial V}{\partial Y}=-\frac{\partial P}{\partial Y}+\frac{1}{\mathrm{Re}}\left(\frac{\partial^2 V}{\partial X^2}+\frac{\partial^2 V}{\partial Y^2}\right)+\frac{\mathrm{Ri}}{\mathrm{Pr}}\beta\theta \tag{11}$$

$$U\frac{\partial \theta}{\partial X}+V\frac{\partial \theta}{\partial Y}=\frac{1}{\mathrm{Re}.\mathrm{Pr}}\left(\frac{\partial^2 \theta}{\partial X^2}+\frac{\partial^2 \theta}{\partial Y^2}\right) \tag{12}$$

In dimensionless forms, local entropy generation can be expressed as following:

$$S^*_{gen}=\frac{1}{(\theta+T^*)^2}\left[\left(\frac{\partial\theta}{\partial X}\right)^2+\left(\frac{\partial\theta}{\partial Y}\right)^2\right]+\frac{1}{(\theta+T^*)}Ec\,\mathrm{Pr}$$
$$\left[2\left\{\left(\frac{\partial U}{\partial X}\right)^2+\left(\frac{\partial V}{\partial Y}\right)^2\right\}+\left(\frac{\partial U}{\partial X}+\frac{\partial V}{\partial Y}\right)^2\right] \tag{13}$$

in which T^*, S^*_{gen}, and Ec are defined as:

$$T^*=\frac{Tc.k_f}{q''.H} \tag{14}$$

$$S^*_{gen}=S_{gen}.\frac{H^2}{k_f} \tag{15}$$

$$Ec=\frac{U_0^2.k_f}{H.Cp_f.q''} \tag{16}$$

In equation (13), the first term on the right-hand side refers to the transfer of heat in the direction of finite temperature gradients and is generally termed as the heat transfer irreversibility (HTI) whilst the second term is the contribution of the fluid friction irreversibility (FFI).

As the distribution of volumetric entropy generation is obtained, it would be integrated over the whole domain to yield the global entropy generation (GEG) rate:

$$S^*_{global}=\iint_{\forall} S^*_{gen}d\forall=\int_0^1\int_0^1 S^*_{gen}dXdY \tag{17}$$

The boundary conditions are in the following forms:

Left vertical wall:

$$\begin{cases}u=v=0\\ \dfrac{\partial T}{\partial x}=0\end{cases}$$

Inlet port:

$$\begin{cases}u=U_0, v=0\\ T=T_c\end{cases}$$

Outlet port:

$$\begin{cases}\dfrac{\partial u}{\partial x}=0, v=0\\ \dfrac{\partial T}{\partial x}=0\end{cases} \tag{18}$$

The bottom horizontal wall:

$$\begin{cases}u=v=0\\ \dfrac{\partial T}{\partial y}=\dfrac{-q''}{k} \quad at \quad y=0\end{cases}$$

The top horizontal wall:

$$\begin{cases}u=v=0\\ \dfrac{\partial T}{\partial y}=0\end{cases}$$

3. Numerical method

The above equations have been solved numerically based on the finite volume method using a collocated grid system. The second order central difference scheme is used to discretize the diffusion terms whereas a mix of upwind and central difference is adopted for the convection terms. The resulting discretized equations have been solved iteratively through strongly implicit procedure (SIP) [24]. The simple algorithm [24] has been adopted for the pressure velocity coupling. More details of the discretization and computational procedure can be found in literatures [25]. To check the convergence of the sequential iterative solution, the sum of the absolute differences of the solution variables between two successive iterations has been calculated. When this summation falls below the convergence criterion which has been choosen as 10-5 in this study, convergence is obtained. We have also used a non-uniform grid mesh which is more appropriate in vicinity of horizontal walls in order to increase the accuracy of the results. Solutions for various mesh sizes have been conducted and the increase in the average Nusselt number as well as the average bulk temperature has been calculated. The results show that the grid system of 73×85 is fine enough to obtain accurate results. Table 1 demonstrates the influence of the number of grid points on the average Nusselt number and the average bulk temperature. At first, the governing equations have been solved for the natural convection flow in an enclosed cavity filled by pure fluid, in order to compare the results with those obtained by de Vahl Davis [26]. This comparison revealed good agreement between results which are shown in Table 2.

4. Result and discussions

The study has been carried out for water working as fluid and the LEG, local FFI, GEG, global HTI, and global FFI are computed. Furthermore, the effects of inlet/outlet ports' location are studied.

Figure 2A shows the LEG, local FFI, isotherm, and streamlines where Ri number is kept constant at 10 in the

Table 1: Results of grid independence examination for the BT configuration

Number of grids in *X-Y*	*Nu*	T_{av}
41×55	17.75000	0.02469
53×65	19.75408	0.02348
61×75	20.63008	0.02330
73×85	20.46283	0.02340
81×95	20.30165	0.02346

Table 2: Comparison of the Nu numbers obtained in this study with those of ref. [26]

Ra	*Nu*		
	present	De Vahl Davis[26]	error
10^4	2.248	2.242	0.267%
10^5	4.503	4.523	0.444%
10^6	9.147	9.035	1.24%

BB configuration. It is well known (Bejan [10-12]) that the heat transfer is due to temperature gradient, fluid friction, and fluid mixing that are three major mechanisms behind entropy generation. For the cavity, the mixing is not present. Considering Fig. 2A, it could be realized that the highest LEG is encountered near the bottom face of the cavity. That is because of the heat flux and consequently the high temperature gradient. The LEG is vanished near the top face of cavity. The LEG is 120 near the bottom wall and decreases in the center of the cavity and approaches to 2×10-7. In the BB configuration and near the bottom wall, the temperature gradient is greater than other places. Therefore, we see the maximum value of LEG near the bottom wall. The local FFI is maximized near inlet and outlet ports and is rather high near walls where the velocities' gradient is greater than other places. The local FFI has the least value at the center of cavity and varies between 1.1×10-5 near the inlet port to 1.6×10-8 at the navel of cavity. The isotherm's figure indicates that the isothermal contour is very high near the bottom face of cavity. The maximum value for isotherms in this case approaches to 0.024, and vanishes in the top and is rather zero in the middle of the cavity. The streamlines are shown at *Ri*=10 and *Ri*=0.1. they show a CCW vortex and at the center of vortex the streamlines' value is maximum and positive. The streamlines' figures show a little change with variation of the Richardson number. Local HTI for 0.1< Richardson number<10 is similar to the local entropy generation in all cases.

Figure 2B displays the above discussed parameter for Richardson number=0.1. The highest LEG value is 0.026, and it occurs near the bottom wall. The value of LEG is zero at the center and the top of the cavity. The isotherm's maximum value is 0.019, and that can be seen near the bottom wall. The LEG contours act similar to isotherm one. The BB configuration's figures show when Richardson number increases the LEG increases as well and that is because of increase in the heat flux. Streamlines and local FFI don't have visible change. The local FFI consists of the both velocity gradients, and the velocities don't show a visible change with increment of the Richardson number. This result will be seen in all cases.

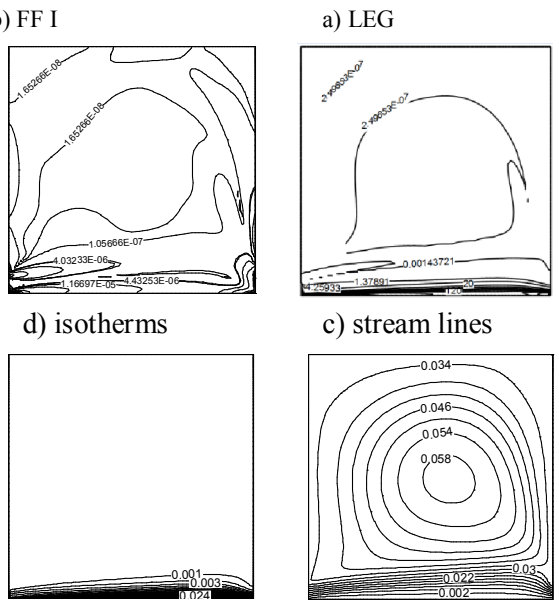

Figure 2A. a) The local entropy generation (LEG), b) local FFI, c) stream lines, and d) isotherms at *Ri*=10 and *Re*=1000 in the BB configuration.

The streamlines can be seen in figures, similar to the BB configuration streamlines, the BT configuration streamlines show a CCW vortex with a maximum and positive value at the center of the cavity.

Figures 3A and 3B display the discussed parameter for the BT configuration at Richardson number 10 and 0.1, respectively. In figure 3A, the highest value of LEG is 100 and its least value is 9×10-7. The LEG is high near the bottom face and rather higher near the right wall because the inclement temperature gradient existed at those positions. The isotherm is high near the bottom wall and rather higher at the right wall and it vanishes far from the bottom and right walls. Its highest value occurred near the bottom wall is 0.05. The highest local FFI located at the inlet port is 1×10-5. The local FFI is high at the inlet port and rather greater near walls and it is zero at the center. At *Ri*=0.1, the highest LEG value is 0.015 and its least value is 2×10-8. The highest value of the isotherm is 0.035 and it is seen near the wall the isotherm vanishes near top and left walls. The streamlines' figure shows a CW vortex and doesn't show a visible change with various Richardson numbers. At the center of the cavity we see the maximum streamlines but that is negative. Also, we can see maximum stremlines near the top and the right walls but that is positive.

Figures 4A and 4B indicate the LEG, FFI, isotherms, and streamlines in the TB configuration at Richardson numbers which are equal to 0.1 and 10, respectively. At *Ri*=10 the maximum value of LEG is 140 and it can be seen near the bottom wall. The LEG is high near the bottom and rather higher near the outlet port and near the left wall. The isotherm's contour is similar to LEG figure and both of them show that the values vanish near the top and right walls. The isotherms' maximum occurs near the

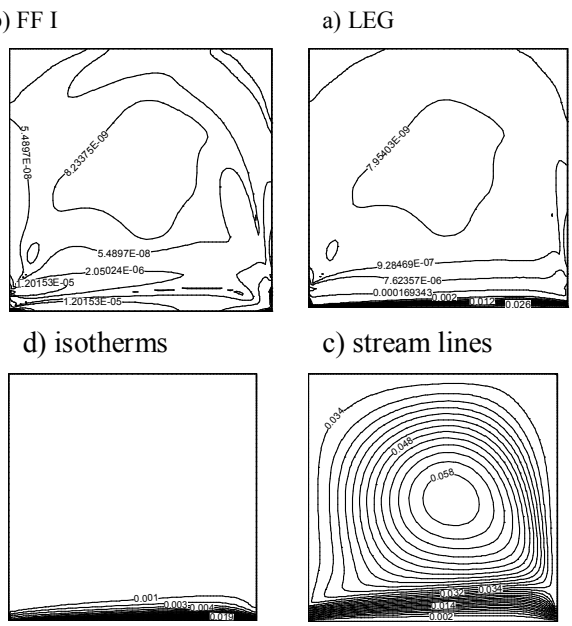

Figure 2B. a) The local entropy generation (LEG), b) local FFI, c) stream lines, and d) isotherms at *Ri*=0.1 and *Re*=1000 in the BB configuration

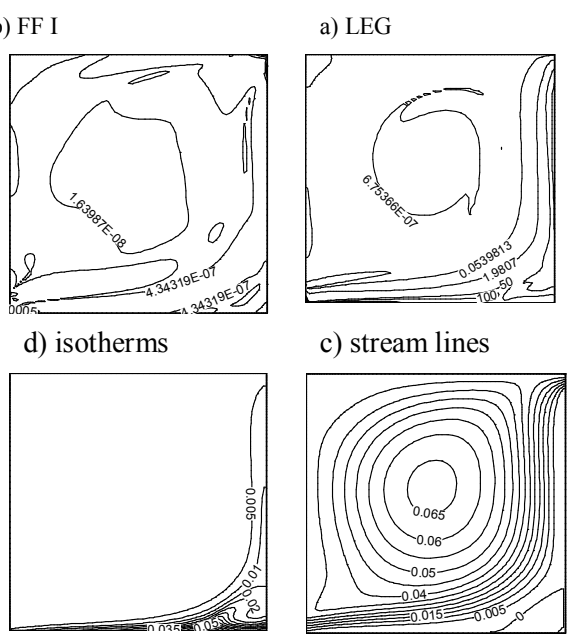

Figure 3A. a) The local entropy generation (LEG), b) local FFI, c) stream lines, and d) isotherms at *Ri*=10 and *Re*=1000 in the BT configuration

bottom wall and is 0.05. The greatest value of the local FFI can be seen at the inlet port. Also, the local FFI is high near walls as well as the outlet port and its value decreases to zero at the center of cavity. At *Ri*=0.1, the LEG varies between 0.026 to 1×10-6. The isotherms' maximum value occurs at the corner between the left and bottom walls and is equal to 0.03. Figure 5A shows the above parameter for the TT configuration at *Ri*=10. The maximum value of LEG can be seen at the inlet port. Also, it is rather high near the bottom wall. The LEG is 135 at the inlet port and it vanishes at the center of cavity, the top wall, and the outlet port. The highest value of isotherm is 0.06. The isotherm is high near the bottom wall and is rather higher near the left wall. The isotherms have a remarkable value at the top of the cavity. The local FFI is maximum at the inlet port with a value equal to 1×10-5. At *Ri*=0.1, the highest LEG value occurs at the bottom wall which is 0.03. The LEG doesn't have a remarkable value at the outlet port and the center of the cavity. The reason of occurring the highest LEG for *Ri*=10 and *Ri*=0.1 at different places could be explained as following: at *Ri*=0.1 the conduction heat transfer is an important term in heat transfer; so, we see the maximum LEG near the bottom wall. At *Ri*=10 the convection heat transfer has a significant role in mixed convection; then, we see the maximum LEG value at the inlet port. The isotherms' maximum value occurs at the bottom and right walls. The streamlines in the TT configuration show a CW vortex. The maximum positive value for streamlines can be seen at the top of the cavity.

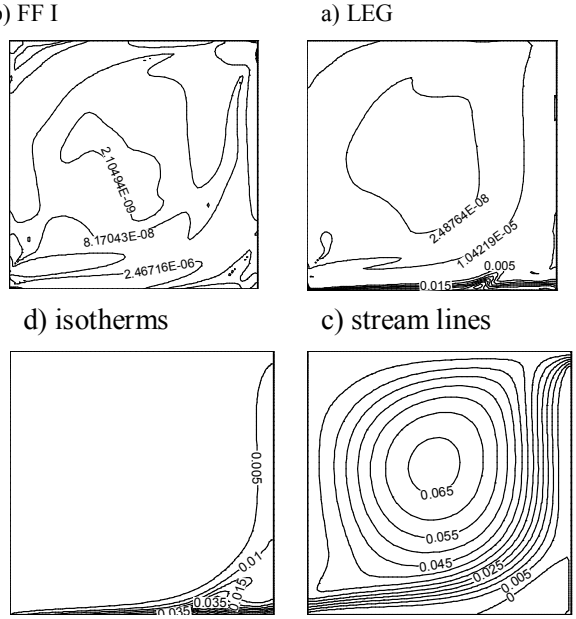

Figure 3B. a) The local entropy generation (LEG), b) local FFI, c) stream lines, and d) isotherms at *Ri*=0.1 and *Re*=1000 in the BT configuration

The result of these four cases at various Richardson number shows:

- LEG increases when the Richardson number is increased.
- The inlet port in the TT configuration has the highest LEG among the other locations. However, in other cases the maximum LEG value is seen in the bottom wall.
- In all cases the local HTI is very similar to LEG.
- In all cases the local FFI is much less than the local HTI. Consequently, in these cases the FFI can be ignored.
- The streamlines and local FFI don't have visible change at various Richardson numbers.

Figure 6 indicates the variety of the global HTI with different Richardson numbers. The Richardson number changes in "0.0001-10" range. The TT configuration has the maximum global HTI value, and that value has a higher growth rate with increasing the Richardson number. Other cases have a rather equal growth rate in global HTI via increment of the Richardson number, especially at high Richardson numbers. The BB configuration has the least global HTI in all cases. In all of these cases, the global HTI increases with increment of the Richardson number.

Figure 7 shows the global FFI for all cases where 0.0001< Richardson< 10. The BB configuration has the least global FFI in all cases. Furthermore, the value of the global FFI has a negative rate by increasing the Richardson number. The BT configuration has a similar trend to the BB configuration but it has a lower negative rate. The TB configuration has the highest global FFI in all cases in the above Richardson number range, and the global FFI increases by increasing the Richardson number similar to the TT configuration. However, the TB configuration has a higher growth rate. The TT and TB have a CW vortex. When the *Ri* number is increased the global FFI increases as well. Nevertheless, the BB and BT have a CCW vortex, the global FFI is decreased. The entropy generation consists of FFI and HTI. At *Ri*>0.001, the global HTI is dominant term in GEG. In the above range of Richardson number the global HTI is much higher than the global FFI. Therefore, the GEG and global HTI almost have equal values. Figure 8 shows the variety of the global entropy generation versus the Richardson number. It shows that the BB configuration has the least GEG.

Figure 9 shows the GEG and global HTI at 0.0001<*Ri*<0.001. In Richardson number=0.0001, the TB has a maximum GEG value, and the BB has the minimum GEG value. The BT configuration's GEG is greater than the TT one. When the Richardson number is increased the GEG of the TT configuration increases with a higher growth rate among all cases. At Richardson=0.001, the GEG of the TT configuration approaches to the GEG of

b) FF I a) LEG

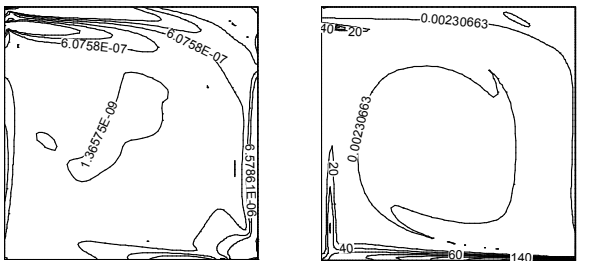

d) isotherms c) stream lines

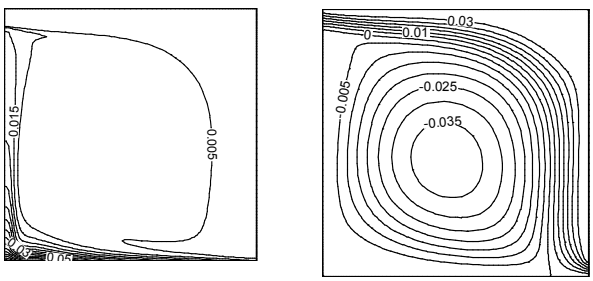

Figure 4A. a) The local entropy generation (LEG), b) local FFI, c) stream lines, and d) isotherms at *Ri*=10 and *Re*=1000 in the TB configuration

b) FF I a) LEG

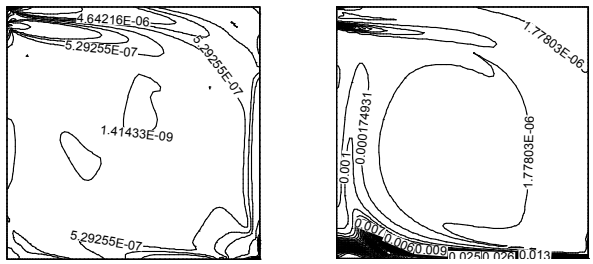

d) isotherms c) stream lines

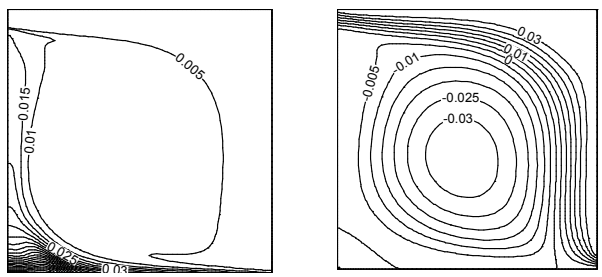

Figure 4B. a) The local entropy generation (LEG), b) local FFI, c) stream lines, and d) isotherms at *Ri*=0.1 and *Re*=1000 in the BT configuration

b) FF I a) LEG

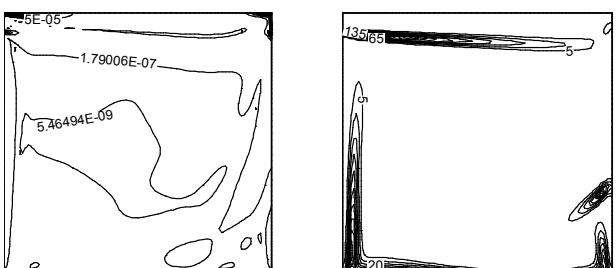

d) isotherms c) stream lines

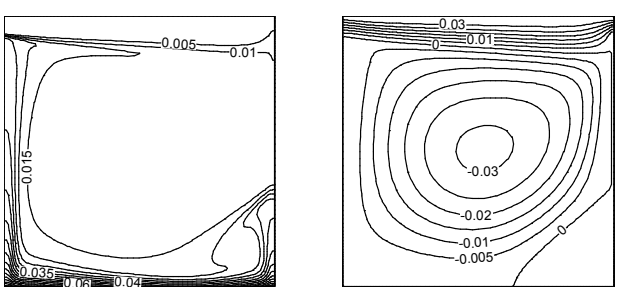

Figure 5A. a) The local entropy generation (LEG), b) local FFI, c) stream lines, and d) isotherms at *Ri*=10 and *Re*=1000 in the TT configuration

b) FF I a) LEG

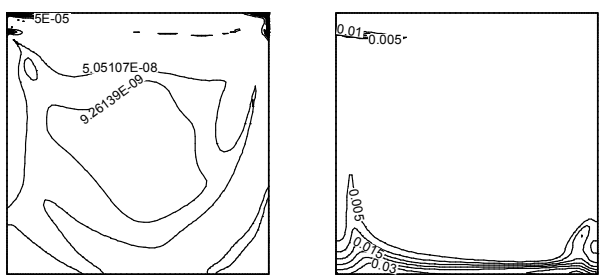

d) isotherms c) stream lines

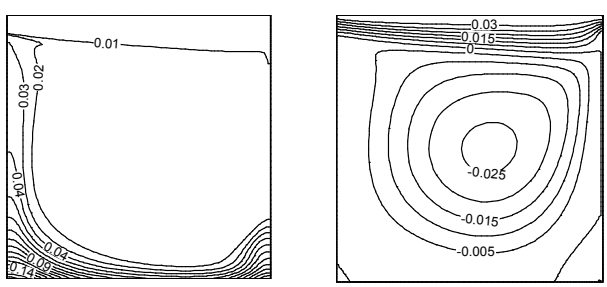

Figure 5B. a) the local entropy generation (LEG), b) local FFI, c) stream lines, and d) isotherms at *Ri*=0.1 and *Re*=1000 in the TT configuration.

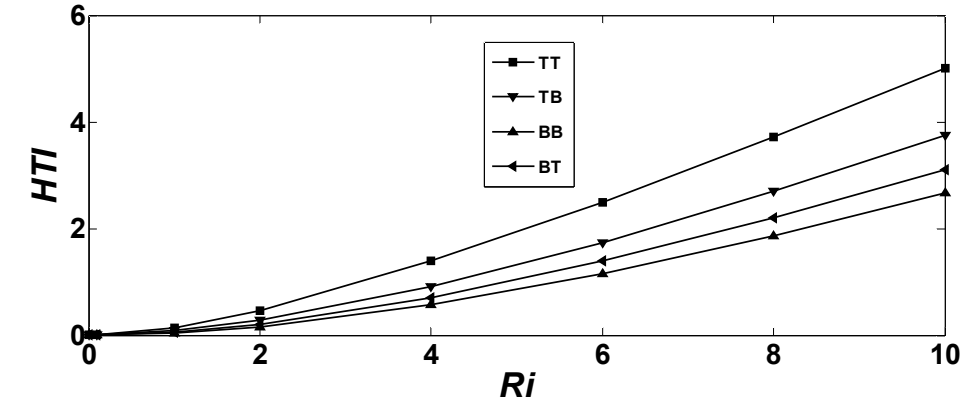

Figure 6. Global HTI vs. the Richardson number

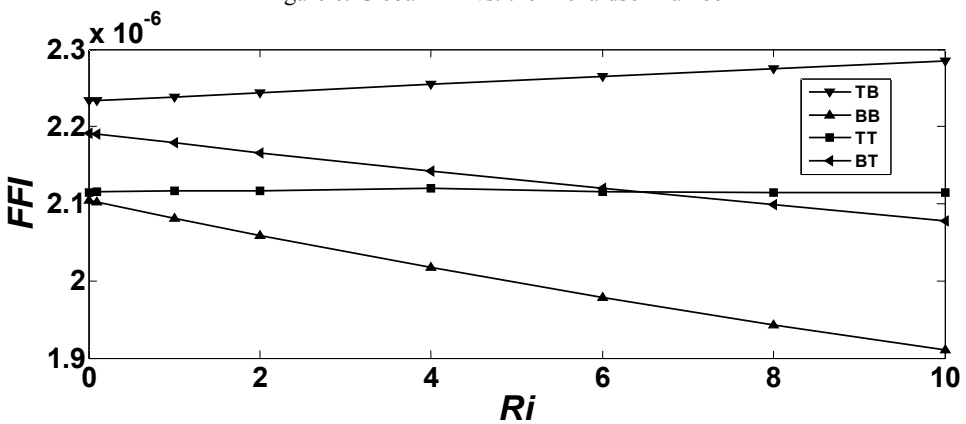

Figure 7. Global FFI vs. the Richardson number

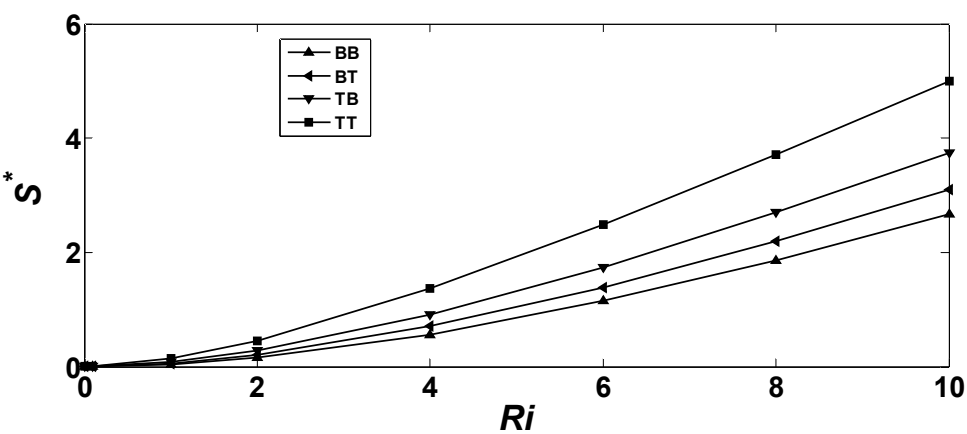

Figure 8. GEG vs. the Richardson number

the TB configuration. Therefore, the TT configuration has the highest GEG with Ri>0.001.

Figure 10 illustrates the average Nusselt number for all cases. In the above range of Richardson number, the average Nusselt number in the TB configuration is the least in all cases. The TB configuration has a small average Nusselt value in comparison with other cases. Other cases almost have a similar average Nusselt number. In the TB and TT configurations when the Richardson Number outgrows to 0.1, the average Nusselt number has a visible growth. Remarkable point in this figure is that the BB configuration's average Nusselt number approaches to the BT configuration's average Nusselt number at high Richardson numbers. The results show that the BB configuration has a maximum heat transfer and minimum

entropy generation. Then, the best configuration is the BB configuration. At low Richardson numbers (10-4<*Ri*<10-4) the TB configuration has a minimum entropy generation value while in higher Richardson numbers (*Ri*>10-3) the TT configuration has the maximum entropy generation value. The TB configuration (in all of Richardson number range) has the minimum heat transfer rate.

5. Conclusion

The effects of inlet and outlet port locations on the mixed convection, HTI, LEG, FFI, and GEG have been investigated. In this study, a cavity with inlet and outlet ports and with a heat source placed on the bottom surface is assumed. In order to investigate the effect of the inlet and outlet locations, four different configurations of the

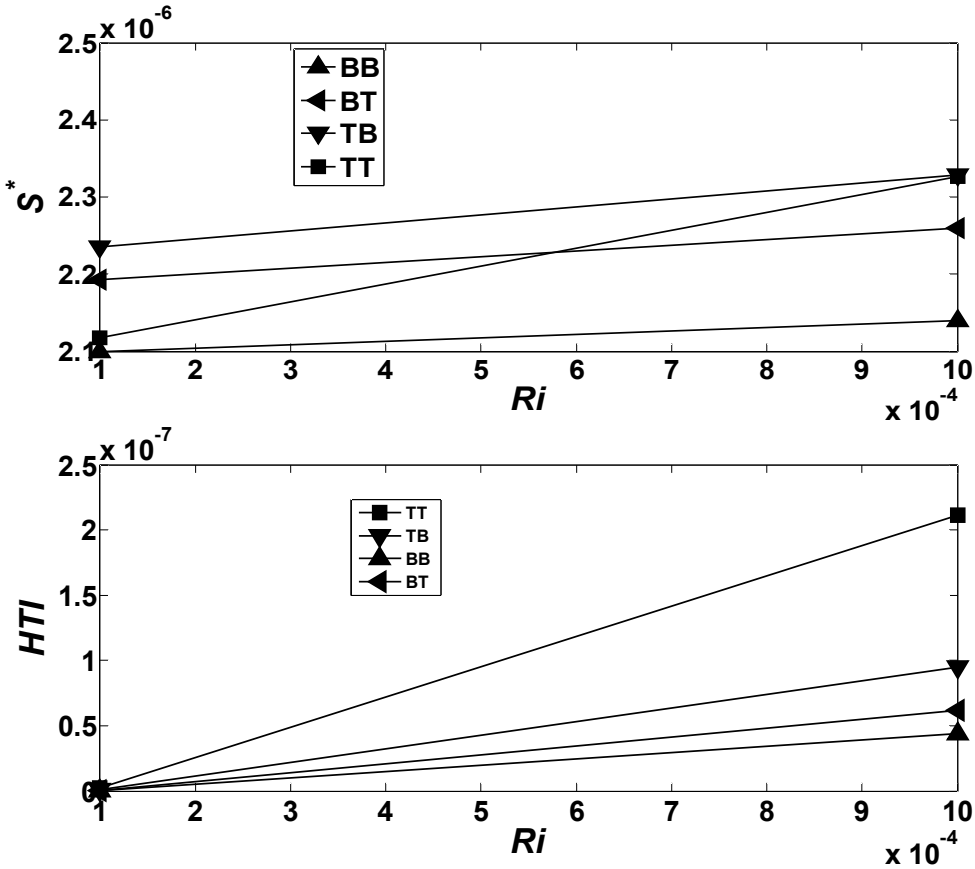

Figure 9. GEG and HTI at 0.0001<Richardson<0.001

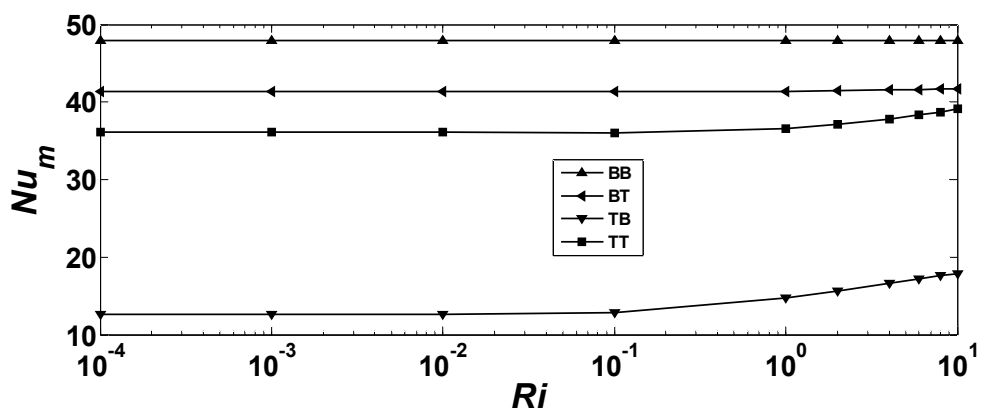

Figure 10. The average Nusselt number vs. the Richardson number

inlet and outlet ports are investigated. The investigation indicates that the Richardson number and port location have an important influence on the LEG and GEG. The inlet port in the TT configuration has the highest LEG between other locations. In other cases, the maximum LEG value is seen on the bottom face. The maximum value of the entropy generation is 140 that occurs near the outlet port in the TB configuration at Ri=10. In all cases, the local FFI is much less than the local HTI. The local FFI vanishes at the center of the cavity. The BB configuration has the least GEG and the highest heat transfer rate between the studied configurations in this study. At 0.001<Ri<10, the TT configuration has the highest GEG while at 0.0001<Ri<0.001 the TB has the highest GEG.

Nomenclature

c_p	Specific heat capacity (J/K)
Gr	Grashof number, $\beta g H^4 q'' / k\upsilon^2$
g	Gravitational acceleration (m/s^2)
H	Height of cavity (m)
P	Dimensionless pressure, $p/\rho_{nf}U_0^2$
p	Pressure (N/m^2)
T	Temperature (K)
k	Thermal conductivity (W/mK)
s	Entropy generation rate (W/m^3K)
Nu	Nusselt number
Re	Reynolds number, $\rho U_0 H/\mu$
Ri	Richardson number, Gr/Re^2
pr	Prandtl number, υ_f/α_f
Ec	Eckert number, $U^2k/H.Cp.q''$
u, v	Components of velocity (m/s)
x, y	Cartesian coordinates (m)
U, V	Dimensionless velocity components, $(U = u/U_0,\ V = v/U_0)$
X, Y	Dimensionless Cartesian coordinates (m)
W	width of cavity (m)
HTI	Heat Transfer Irreversibility
FFI	Fluid Friction Irreversibility
GEG	Global Entropy Generation
LEG	Local Entropy Generation
CCW	Counter clock wise
Greek letters	
α	Thermal diffusivity, $k/(\rho c_p)$ (m^2/s)
β	Coefficient of volume expansion (K^{-1})
μ	Dynamic viscosity (Pa.s)
υ	Kinematics viscosity (m^2/s)
ρ	Density (kg/m^3)
θ	Dimensionless temperature
Subscript	
c	Reference (ambient)
f	Fluid
m	Average
w	Wall

References

[1]. K.J. Kennedy, A. Zebib, Combined free and forced convection between horizontal parallel planes: some case studies, Int. J. Heat Mass Transf., 26, 471–474 (1983).

[2]. T. Basak, S. Roy, P.K. Sharma, I. Pop, Analysis of mixed convection flows within a square cavity with uniform and non-uniform heating of bottom wall, Int. J. Therm. Sci., 48, 891–912 (2009).

[3]. G. Guo, M.A.R. Sharif, Mixed convection in rectangular cavities at various aspect ratios with moving isothermal sidewalls and constant flux heat source on the bottom wall, Int. J. Therm. Sci., 43, 465–475 (2004).

[4]. K.M. Khanafer, A.M. Al-Amiri, I. Pop, Numerical simulation of unsteady mixed convection in a driven cavity using an externally excited sliding lid, Eur. J. Mech. B/Fluids, 26, 669–687 (2007).

[5]. S. Saha, G. Saha, M. Ali, Md.Q. Islam, Combined free and forced convection inside a two-dimensional multiple ventilated rectangular enclosure, ARPN J. Eng. Appl. Sci., 1 (3), 23–35 (2006).

[6]. M.D.M. Rahman, M.A. Alim, S. Saha, M.K. Chowdhury, A numerical study of mixed convection in a square cavity with a heat conducting square cylinder at different locations, J. Mech. Eng., ME39 (2), 78–85 (2008).

[7]. B. Ghasemi, S.M. Aminossadati, Numerical simulation of mixed convection in a rectangular enclosure with different numbers and arrangements of discrete heat sources, Arab. J. Sci. Eng., 33 (1B), 189–207 (2008).

[8]. S. Saha, G. Saha, M. Ali, Md.Q. Islam, Combined free and forced convection inside a two-dimensional multiple ventilated rectangular enclosure, ARPN J. Eng. Appl. Sci., 2 (2), 25–36 (2007).

[9]. A. H. Mahmoudi, M. Shahi, F. Talebi, Effect of inlet and outlet location on the mixed convective cooling inside the ventilated cavity subjected to an external nanofluid, Int. Comm. Heat Mass Transfer, 37, 1158-1173 (2010).

[10]. A. Bejan, A study of entropy generation in fundamental convective heat transfer, J. Heat Transfer, 101, 718-725 (1979).

[11]. A. Bejan, Second-law analysis in heat and thermal design, Adv. Heat Transfer, 15, 1-58 (1982).

[12]. A. Bejan, Entropy Generation Minimization, CRC press, Boca Raton, NY, (1996).

[13]. N. Kasagi, M. Nishimura, DNS of combined forced and natural convection in a vertical plane channel, Int. J. Heat Mass Transfer, 18, 88-99 (1997).

[14]. A.C. Baytas, Entropy generation for natural convection in an inclined porous cavity, Int. J. Heat Mass Transfer, 43, 4225-4232 (2000).

[15]. S. Mahmud, R. A. Fraser, The second-law analysis in fundamental convective heat transfer problem, Int. J. Thermal Sciences, 42, 177-186 (2003).

[16]. A. Andreozzi, A. Auletta, O. Manca, Entropy generation in natural convection in a symmetrically and uniformly heated vertical channel, int. J. Heat Mass Transfer, 49, 3221-3228 (2006).
[17]. A.Omri, and S.B. Nasrallah, Control volume finite element numerical simulation of mixed convection in an air-cooled cavity, Numerical Heat Transfer, Part A, 36, 615-637 (1999).
[18]. S. Singh, and M.A.R. Sharif, Mixed Convection cooling of a rectangular cavity with inlet and exit openings ondifferentially heated side walls. Numerical Heat Transfer, Part A, 44, 233-253(2003).
[19]. Md. Mustafizur Rahman, M. A. Alim and Sumon Saha, mixed convection in a square cavity with a heat-conducting horizontal square cylinder, Suranaree J. Sci. Technol., 17,139-153 (2010).
[20]. C. Balaji, M. Holling, H. Herwing, Entropy generation minimization in turbulent mixed convection flows, Int. Comm. Heat Mass Transfer, 34, 544-552 (2007).
[21]. I. Zahmatkesh, on the importance of thermal boundary conditions in heat transfer and entropy generation for natural convection inside a porous enclosure, Int. J. Thermal Sciences, 47, 339-346 (2008).
[22]. M. shahi, A.H. Mahmoudi, A. Honarbakhsh Rauof, entropy generation due to a natural convection cooling of nanofluid, Int Comm. Heat Mass Transfer, 38, 972-983 (2011).
[23]. A. H. Mahmoudi, I. Pop, M. Shahi, F. Talebi, MHD natural convection and entropy generation in a trapezoidal enclosure using nanofluid, computer and fluids, 72, 46-62 (2013).
[24]. J.H. Ferziger, M. Peric, Computational Method for Fluid Dynamic, Springer-Verlag, NY, (1999).
[25]. S.V. Patankar, Numerical heat transfer and fluid flow, hemisphere, NY, (1980).
[26]. G. De Vahl Davis, Natural convection of air in a square cavity a bench mark numerical solution, Int. J. Numer. Meth. Fluids, 3, 249–264 (1983).